The 46th Annual Conference of the IEEE Industrial Electronics Society - IECON 2020

Highly Flexible Indirect Modular Multilevel Converter for High Power Pumped Hydro Storage Plants

M. Basic, A. Schwery, and D. Dujic

POWER ELECTRONICS LABORATORY
ÉCOLE POLYTECHNIQUE FÉDÉRALE DE LAUSANNE

Highly Flexible Indirect Modular Multilevel Converter for High Power Pumped Hydro Storage Plants

Miodrag Basić
Power Electronics Laboratory
EPFL
CH-1015 Lausanne, Switzerland
miodrag.basic@epfl.ch

Alexander Schwery
engineering/technology
GE Renewable Energy
CH-5242 Birr, Switzerland
alexander.schwery@ge.com

Dražen Dujić
Power Electronics Laboratory
EPFL
CH-1015 Lausanne, Switzerland
drazen.dujic@epfl.ch

***Abstract*—As fossil-fuel- and nuclear-based generating facilities are being phased-out in favor of intermittent renewable energy sources, the need for large scale, highly flexible balancing storage is imminent. By the generating capacity of readily available units, enormous potential lays in retrofitting of large pumped hydro storage plants to variable speed operation, increasing their flexibility to meet future power system demands. Indirect Modular Multilevel Converter is a highly scalable and inherently redundant topology that meets the power and voltage ratings of large pumped hydro generating units. Variable DC link converter operation, offering common-mode-free machine-side operation has been evaluated, considering constraints in retrofit of old machines, not designed for converter-fed operation. Performance evaluation over the entire operating range of the plant is performed. Grid support dynamics has been assessed. Finally, application-specific challenges in the design stage are pointed out.**

***Index Terms*—Indirect MMC, MV, Pumped Hydro**

I. Introduction

For considerable time now, power systems are seeing persistent increase in installed Renewable Energy Sources (RES) generation capacities, predominantly Photo-Voltaic (PV) and wind turbines. As we are heading towards RES-dominated power systems, the need for high-volume highly-flexible energy storage systems, that would counter-weight the intermittent nature of these sources, is imminent. With the highest share of grid-scale installed capacity and minute-range start-up times, large (Tab. I) Pumped Hydro Storage Plants (PHSPs) already offer significant balancing potential.

Variable Speed (VS) PHSPs offer further flexibility through variable pumping power, i.e. grid frequency control in both pumping and generating modes of operation. This is essential as the excess of energy produced by non-dispatchable RES can be balanced, while eliminating the need for fossil-fuel-based units [1], [2]. Further efficiency increase through the selection of optimal operating speed [3], and increased revenue from participating at ancillary services market [4], are clear motivations for retrofit of existing PHSP units to VS.

TABLE I: Typical machine ratings in large PHSPs

Stator voltage	V_{LL}	6 kV to 21 kV
Stator current	I_{RMS}	2 kA to 8 kA
Apparent power	S_n	80 MVA to 400 MVA

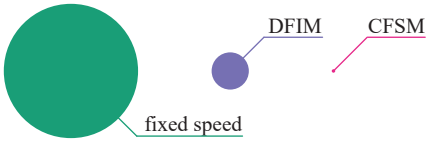

Fig. 1: Share of VS DFIM (≈10 GW) and CFSM (0.1 GW) units larger than 100 MW, compared to total installed PHSP generating capacity (≈160 GW) [6], [7].

Historically, components- and topologies-related limitations in available power electronics converters restricted large VS units to the use of Doubly-Fed Induction Machine (DFIM) (Fig. 1), with only one Converter-Fed Synchronous Machine (CFSM)-based VS-retrofitted unit in operation [5].

Significant potential lays in retrofit of existing fixed speed PHSPs to CFSM-based VS units. While keeping the original machine, CFSM enables turbine/pump change-over without de-watering, grid-side dynamical behaviour only limited by the fast current control loops, Low-Voltage Ride-Through (LVRT) handling superior to DFIM, with full control over the fault current and grid support. However, unlike [5], a highly scalable design is necessary to mitigate the need for additional voltage matching transformers.

Considering machine ratings from Tab. I, Modular Multilevel Converter (MMC) topology is a good candidate, due to the unrestricted power and voltage scalability and inherent redundancy [7]. In AC-AC applications, such is a grid-connected drive of the PHSP, either a matrix-like Direct MMC (D-MMC), or a back-to-back Indirect MMC (I-MMC) can be considered. D-MMC is an efficient solution if machine- and grid-frequency differ, making it suitable for new installations, with unrestricted choice of machine parameters [8].

I-MMC decouples AC systems of the machine and the grid, being suitable for arbitrary ratio of machine- and grid-frequency, including equal values. This is essential for retrofit of existing fixed speed PHSP units, where ideally no modifi-

978-1-7281-5413-8/20/$31.00 ©2020 IEEE

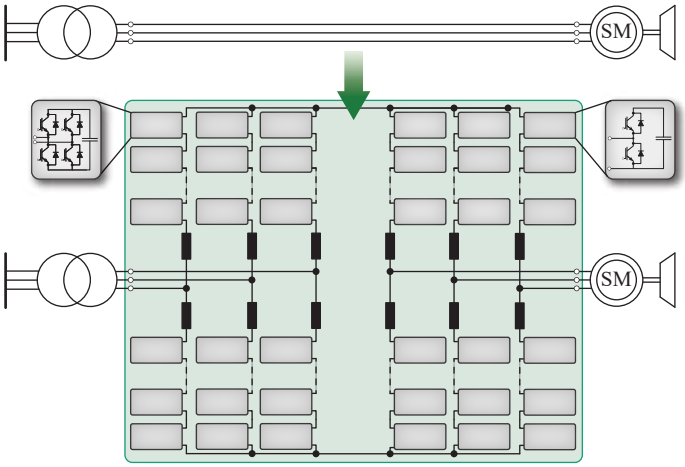

Fig. 2: Retrofit of an existing PHSP with I-MMC for conversion to VS operation, without machine modifications.

cations to the machine should occur (Fig. 2).

As shown in literature, topology-specific requirements exist when supplying VS electric machines from MMC [9]. The additional machine stress that these methods impose, in terms of high Common Mode (CM) voltage amplitudes at Low Frequency (LF), up to rated winding voltage, can prove prohibitively high when retrofitting units that were originally designed for sine-wave grid supply.

Research community has recognized the potential in variable DC link voltage operation of machine-side MMC stage. In [10], a switch is introduced to the DC link, voltage from an ideal DC source is chopped to achieve appropriate average V_{DC}. The entire converter reliability, however, relies on the newly introduced switch, thus redundancy is compromised. A two-quadrant solution is proposed in [11], utilizing Cascaded H-Bridge (CHB) as the grid-side stage. In [12], hybrid grid-side MMC stage is proposed, while two fixed-frequency operating points of the machine were observed. The use of Full-Bridge (FB) grid-side MMC stage is discussed to some extent in [13]. However, only open-loop V/f controlled machine ramp-up was observed at the limited frequency range.

This paper extends the analysis of variable DC link MMC operation, enabled through the use of FB Submodules (SMs) on the grid side, offering an I-MMC-based solution specially suitable for, but not limited to, retrofit of existing PHSPs to highly flexible VS operation. No existing equipment modification should be required, while high gains are obtained in terms of PHSP response and grid support functionality.

II. Low frequency CM-free operation

Owing to the use of scalability-enabling two-terminal SMs, comprising floating voltage capacitors, as MMC building blocks, their state-of-charge dynamics must be analyzed over the entire PHSP operating range to ensure proper operation.

A. Machine-side stage

Machine-side MMC considers realization based on Half-Bridge (HB) SMs (Fig. 2), which is sufficient for inverter operation. This stage should allow for:

- Zero-speed controlled start in pump or turbine mode.
- Variable speed operation up to rated speed.
- Seamless switch-over between pump and turbine operating modes, to an extent allowed by the hydraulic system.

Assuming ideally balanced converter, i.e. no balancing current components, and no CM voltage applied, instantaneous branch power can be analyzed.

$$p_{\{\mathrm{p,n}\}\mathrm{x}} = v_{\{\mathrm{p,n}\}\mathrm{x}} i_{\{\mathrm{p,n}\}\mathrm{x}} \tag{1}$$

where $i_{\{\mathrm{p,n}\}\mathrm{x}} = i_{\mathrm{cx}} \pm i_{\mathrm{sx}}/2$, $v_{\{\mathrm{p,n}\}\mathrm{x}} = v_{\mathrm{cx}} \mp v_{\mathrm{sx}}$. The following notation is adopted: $\{\mathrm{p,n}\}$ – upper/lower branch, $x \in \{\mathrm{a,b,c}\}$ – phase, $v_{\mathrm{c}} = (v_{\mathrm{n}} + v_{\mathrm{p}})/2$ – total inserted leg voltage, $v_{\mathrm{s}} = (v_{\mathrm{n}} - v_{\mathrm{p}})/2$ – differential leg voltage, $i_{\mathrm{c}} = (i_{\mathrm{p}} + i_{\mathrm{n}})/2$ – circulating current, $i_{\mathrm{s}} = i_{\mathrm{p}} - i_{\mathrm{n}}$ – AC-terminal current. The choice of observed converter branch is irrelevant for the analysis, thus upper branch of phase *a* is observed, i.e. $\{\mathrm{p,n}\}\mathrm{x} = \mathrm{pa}$, subscript being omitted.

$$i_{\mathrm{c}} = \frac{I_{\mathrm{dc}}}{3} \qquad i_{\mathrm{s}} = \hat{i}_{\mathrm{s}} \cos(\omega_s t - \varphi) \tag{2}$$

$$v_{\mathrm{c}} = \frac{V_{\mathrm{dc}}}{2} \qquad v_{\mathrm{s}} = m_s \frac{V_{\mathrm{dc}}}{2} \cos(\omega_s t) \tag{3}$$

where m_s denotes AC voltage modulation index. Substituting (2) and (3) to (1), while assuming $v_{\mathrm{SM}} = v_{\mathrm{pa}}/N_{\mathrm{SM}}$, instantaneous SM-level active power is derived, and non-zero- and zero-average members can be identified.

$$\begin{aligned} p_{\mathrm{SM}} = {} & \underbrace{\frac{V_{\mathrm{dc}} I_{\mathrm{dc}}}{6N_{\mathrm{SM}}}}_{P_{\mathrm{dc,SM}}} - \underbrace{m_s \frac{V_{\mathrm{dc}} \hat{i}_{\mathrm{s}}}{8N_{\mathrm{SM}}} \cos(\varphi)}_{P_{\mathrm{ac,SM}}} \\ & + \frac{V_{\mathrm{dc}}}{N_{\mathrm{SM}}} \Bigg\{ \underbrace{\frac{\hat{i}_{\mathrm{s}}}{4} \cos(\omega_s t - \varphi)}_{\text{zero average}} - \underbrace{m_s \frac{I_{\mathrm{dc}}}{6} \cos(\omega_s t)}_{\text{zero average}} \\ & \underbrace{- m_s \frac{\hat{i}_{\mathrm{s}}}{8} \cos(2\omega_s t - \varphi)}_{\text{zero average}} \Bigg\} \end{aligned} \tag{4}$$

To prevent average SM energy deviation, average SM-level active power of (4) must equal zero, i.e. $P_{\mathrm{dc,SM}} = P_{\mathrm{ac,SM}}$. Normally only average energy values are balanced in MMC, oscillating components (5) being buffered by SM capacitors.

$$\begin{aligned} \tilde{w}_{\mathrm{SM}} = \int \tilde{p}_{\mathrm{SM}} \, \mathrm{d}t = \frac{V_{\mathrm{dc}} \hat{i}_s}{4N_{\mathrm{SM}}} \Bigg\{ & \underbrace{\frac{1}{\omega_s} \sin(\omega_s t - \varphi)}_{\text{(I) decreases with } \omega_s} \\ & \underbrace{- \frac{m_s^2}{2\omega_s} \cos(\varphi) \sin(\omega_s t)}_{\text{(II) increases with } \omega_s} \underbrace{- \frac{m_s}{4\omega_s} \sin(2\omega_s t - \varphi)}_{\text{(III) constant}} \Bigg\} \end{aligned} \tag{5}$$

Assuming constant-torque CFSM operation, as the worst-case scenario for the analysis, machine-side SM energy ripple behaviour can be characterized over the entire operating speed range of the machine, $(0 \ldots \omega_{\mathrm{s,rated}}]$, following (6).

$$\hat{i}_s \approx \text{const.} \qquad \hat{v}_s/\omega_s \approx \text{const.} \qquad \hat{v}_s = m_s V_{\mathrm{dc}}/2 \tag{6}$$

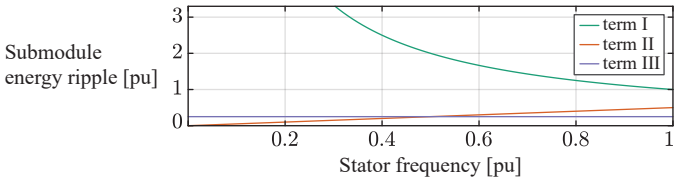

Fig. 3: Frequency dependence of SM energy ripple components (5). The first term is dominant in LF region.

where i_s, v_s and ω_s denote stator current, voltage and angular frequency, respectively.

Amplitudes of three SM energy ripple members (5) manifest different dependencies on output frequency (Fig. 3). The first member is proportional to $1/\omega_s$, having dominant influence in LF region. The second member is proportional to m_s^2/ω_s and, considering (6), approximately linearly increases with the output frequency. The third member is proportional to m_s/ω_s, thus having constant value, according to (6).

Setting branch-level sum capacitor voltage reference to rated DC link voltage (7), while assuming equal voltage distribution between SMs, SM capacitor voltage ripple is derived (8) for the dominant first term of (5).

$$v^*_{\mathrm{C}\Sigma} = V_{\mathrm{DC,rated}} = N_{\mathrm{SM}} V_{\mathrm{SM}} \tag{7}$$

$$\begin{aligned}\Delta\tilde{w}_{\mathrm{SM}} &= \frac{C_{\mathrm{SM}}}{2}\left(\left(V_{\mathrm{SM}}+\Delta v_{\mathrm{SM}}\right)^2 - \left(V_{\mathrm{SM}}-\Delta v_{\mathrm{SM}}\right)^2\right) \\ &= 2C_{\mathrm{SM}} V_{\mathrm{SM}} \Delta v_{\mathrm{SM}}\end{aligned} \tag{8}$$

Substituting (7) and first member of (5) to (8) leads to:

$$\Delta v_{\mathrm{SM,dom,lf}} = \frac{V_{\mathrm{DC}}\hat{i}_s}{8V_{\mathrm{DC,rated}}C_{\mathrm{SM}}\omega_s}\sin(\omega_s t-\varphi) \tag{9}$$

where $\hat{i}_s$ is constant for constant torque, while C_{SM} and $V_{\mathrm{DC,rated}}$ are fixed by design. As DC link voltage is a purely internal I-MMC quantity, setting $V_{\mathrm{DC}} \neq V_{\mathrm{DC,rated}}$, such that:

$$V_{\mathrm{DC}} = k_{\mathrm{DC}} V_{\mathrm{DC,rated}} \qquad k_{\mathrm{DC}}/\omega_s = \text{const.} \tag{10}$$

SM voltage ripple (9) is constant irrespective of operating frequency, without augmentation of C_{SM} and without the introduction of CM voltage injection as in [9]. In an all-HB I-MMC, however, the lowest attainable DC link voltage is limited by the grid voltage amplitude, allowing only for slight reduction below $V_{\mathrm{DC,rated}}$ value. To enable CM-free operation through (10), FB-based grid-side stage is proposed, allowing $V_{\mathrm{DC}} \in [-V_{\mathrm{DC,rated}}, V_{\mathrm{DC,rated}}]$ DC link voltage range.

Recalling (3) and (10), if the DC link voltage is to be reduced, modified branch voltage reference is obtained.

$$v_{\{\mathrm{p,n}\}\mathrm{SM}} = \frac{V_{\mathrm{dc}}}{2}\left(k_{\mathrm{DC}} \mp m_{\mathrm{s,SM}}\cos\left(\omega_{\mathrm{s,SM}}t\right)\right) \tag{11}$$

As full speed range is required, while at LF $\hat{v}_s/\omega_s \neq$ const. (6), recalling (10), k_{DC} is determined (12) to always satisfy Field-Oriented Control (FOC)-generated stator voltage reference without driving (11) negative, assuming $m_{\mathrm{s,SM}} \in [0,1]$.

$$k_{\mathrm{DC}} = m_{\mathrm{s,SM}} \tag{12}$$

B. Grid-side stage

Variable DC link voltage operation, in $V_{\mathrm{DC}} \in [0, V_{\mathrm{DC,rated}}]$ range of (12), is enabled through the use of bipolar FB SMs in the grid-side stage, as presented in Fig. 2. Analogously to (11), grid-side branch voltage reference is obtained.

$$v_{\{\mathrm{p,n}\}\mathrm{grid}} = \frac{V_{\mathrm{dc}}}{2}\left(k_{\mathrm{DC}} \mp m_{\mathrm{s,grid}}\cos\left(\omega_{\mathrm{s,grid}}t\right)\right) \tag{13}$$

While definitely being a more costly solution compared to an all-HB I-MMC where machine-stage is operated as [9], the proposed topology offers sine-wave-alike supply to the machine, without prohibitively-high-amplitude CM voltage, over the entire frequency range. Existing machines can thus be kept in operation with no modifications, which is significant considering Tab. I ratings.

III. Converter Control

Higher-level control system of the proposed converter for a VS PHSP, developed in compliance with control schemes utilized in the existing VS PHSPs [14], is outlined in Fig. 4.

Transmission System Operator (TSO)-scheduled active and reactive power references are, if necessary, scaled by Grid Code (GC)-defined frequency- and voltage-support functions $P(f_g)$ and $I_Q(v_g)$ [15]. If both support actions are simultaneously required, advantage can be given to either of them, by scaling of the lower-priority one according to converter current limit. Reactive power is given advantage here.

A. Grid-side higher-level control

Active Front-End (AFE) stage has dual role. Firstly, exchange of reactive energy with the grid is performed according to TSO schedule, GC, or contracted ancillary service, regardless of the Wound-Rotor Synchronous Machine (WRSM) operating state. GC-scaled reactive power reference Q^*_{grid} is fed to the Grid Current Control (GCC).

Secondly, DC link voltage is controlled through active energy exchange with the grid, at reference P^*_{grid}, equal to GC-scaled P^*_{SM}, slightly augmented to supply converter losses.

B. Machine-side higher-level control

Inverter Unit (INU) stage exchanges active energy with the hydraulic system at GC-scaled reference P^*_{SM} – pumping or

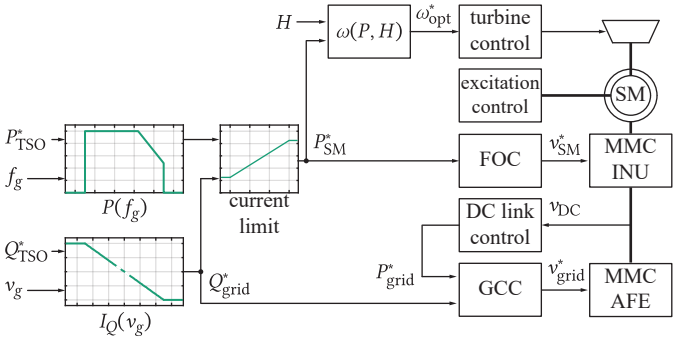

Fig. 4: Overview of the complete control system structure of the proposed converter.

TABLE II: Medium voltage WRSM parameters, model SEVER RMSOT 6355 Lk-4, used in the scaled down setup.

Parameter	Symbol	Value
Apparent power	S_n	0.526 MVA
Active power	P_n	0.5 MW
Torque	M_n	3044 N m
Stator voltage	$V_{\mathrm{s,n}}$	6.3 kV (star)
Stator current	$I_{\mathrm{s,n}}$	48 A
Speed/frequency	$\omega_{\mathrm{e,n}}$	1500 min^{-1} / 50 Hz
Excitation current	$I_{\mathrm{f,max}}$	16 A
Excitation voltage	$V_{\mathrm{f,max}}$	262 V

generating, at arbitrary power factor (unity in this case), as it is decoupled from the grid.

P^*_{SM} and water head H are fed to an algorithm that outputs optimal machine speed for highest hydraulic system efficiency. Turbine controller operates guide vanes following ω^*_{opt}. Based on P^*_{SM} and instantaneous WRSM speed, FOC performs machine torque control. Dynamics of response to the P^*_{SM} change is thus determined by fast machine current control.

WRSM excitation controller is operated in the constant flux mode up to the rated speed, with the possibility of field-weakening operation should the speed above rated be required.

C. Internal MMC control

Energy balancing control loops are implemented equally in both INU and AFE stage, the only difference being in total energy control – while INU is supplied from the DC link, AFE is supplied from the grid. The first method from [16] is used, as it provides superior reaction times at the expense of slightly higher circulating current amplitudes. Phase-Shifted Carrier PWM (PSC-PWM) modulation method is implemented.

IV. Test scenario

Two test scenarios have been defined, aiming to cover the typical PHSP operating sequences under normal grid conditions, as well as LVRT during worst-case voltage drop.

A. Ratings

Evaluation of the proposed solution has been assessed through high-fidelity simulations of a scaled down Medium-Voltage (MV) 0.5 MVA system, adopting parameters of the actual PHSP emulation platform being developed in our laboratory [7]. WRSM ratings are provided in Tab. II, while converter data is presented in Tab. III.

SM voltage ripple limit of $\pm 10\,\%$ is adopted, at total energy of $84.4\,\mathrm{J/kVA}$ per MMC stage (Tab. III). This is in accordance with the analysis in [9], where ripple limit just below $\pm 20\,\%$ was obtained at $42\,\mathrm{J/kVA}$ of stored energy per stage.

B. VS PHSP operation

Test scenario sequence is presented in Fig. 5. Machine torque is kept constant at $90\,\%$ of rated value. Speed reference is varied from standstill, to positive rated, followed by change of direction (i.e. operating mode) under constant torque. WRSM is operated at unity power factor, while grid-side reactive power reference is varied in the range of $-20\,\%$ to $20\,\%$ of apparent power (Tab. III).

TABLE III: I-MMC parameters, based on the prototype being developed [7].

Parameter	Symbol	Value
Line voltage	U_{n}	6.3 kV
Apparent power	S_{n}	0.5 MVA
Grid frequency	f_{n}	50 Hz
Number of SMs per branch	N_{SM}	16
SM voltage	V_{SM}	625 V
SM capacitance (tolerance $\pm 5\%$)	C_{SM}	2.25 mF
Branch inductance	L_{br}	2.5 mH
Branch inductance coupling coeff.	k_{br}	0.3
Branch resistance	R_{br}	20 mΩ
Switching frequency	f_{sw}	999 Hz

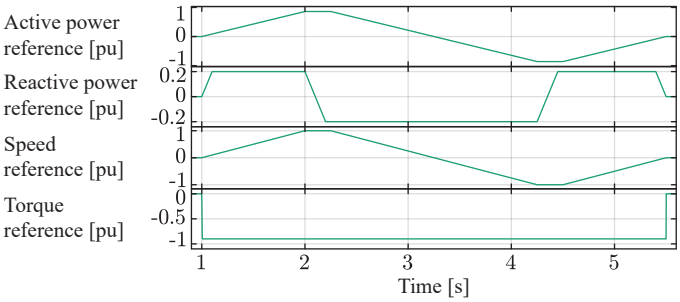

Fig. 5: Test scenario reference values, top to bottom: grid-side active power (0.9 pu), grid-side reactive power (0.2 pu), PHSP speed reference (−1 pu to 1 pu), WRSM torque (−0.9 pu).

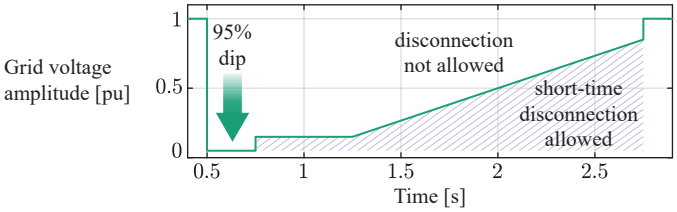

Fig. 6: Worst case grid-code-defined limiting curve for a generating facility of Type 2, adapted from [15]. Generating units must ride through the fault without disconnection for all the cases above the solid line.

C. LVRT evaluation

LVRT capability of the proposed design has been evaluated for the worst case GC-defined scenario [15], for Type 2 generating facility, i.e. plant connected to the grid trough a converter, presented in Fig. 6.

V. Simulation results

A. Machine-side VS PHSP operation

Machine-side stage sequence of operation, corresponding to Fig. 5 test scenario, is presented in Fig. 7. Constant torque reference is correctly tracked over the entire speed range, including zero crossing. As DC link voltage is now varied

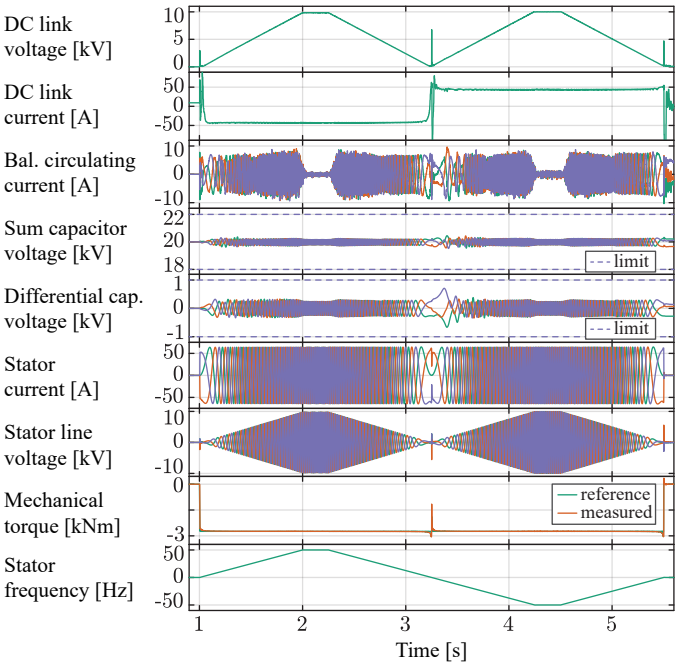

Fig. 7: Machine-side MMC full cycle of opeartion according to the test scenario of Fig. 5.

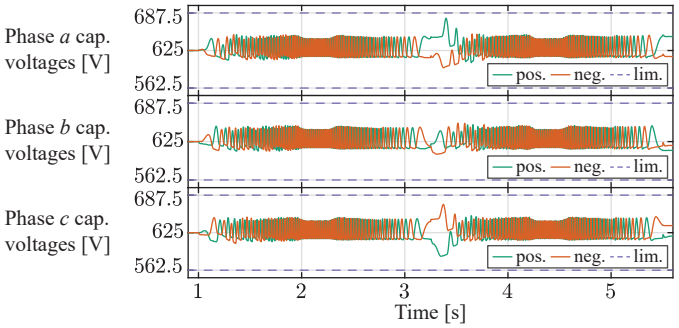

Fig. 8: Per-phase capacitor voltage ripple of the machine-side MMC stage, for Fig. 5 test profile.

proportional to speed, DC current is constant. Significant transients expectedly occur during step-change in i_{DC} reference, caused by step change in torque reference at $t \in \{1\,\mathrm{s}, 5.5\,\mathrm{s}\}$ and by P^*_{SM} sign change-over at zero speed crossing, causing step change of sign in i_{DC} at $t \approx 3.25\,\mathrm{s}$. Both sum and differential capacitor voltage ripple are constant over the entire frequency range, with the exception of an overshoot occurring at zero crossing, around $t = 3.25\,\mathrm{s}$.

B. Zero-crossing capacitor ripple

As the simulation results confirm, machine-side SM capacitor ripple is indeed constant at frequencies down to zero. However, right after frequency zero-crossing, Fig. 8 shows a significant rise in capacitor voltage of the upper branches of phases *a* and *c* occurs at $t = 3.35\,\mathrm{s}$. This transient cannot be evaluated assuming sinusoidal waveform of (5), but rather by observing instantaneous voltage and current state of a SM, given for phase *a* in Fig. 9.

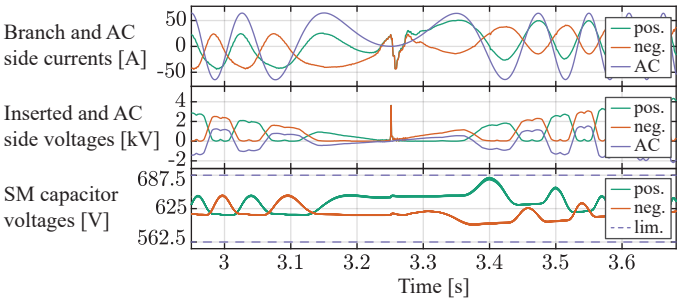

Fig. 9: Phase *a* transient is presented, for zero-speed crossing under constant torque. A low-amplitude third harmonic voltage is injected for better DC link utilization. Lowermost graph presents an envelope of all SM capacitors' voltage, colour-coded to upper and lower branch.

Approaching zero speed at sinusoidal voltage and current waveforms, Δv_{SM} is constant, according to (9). During $t \in [3.25\,\mathrm{s}, 3.35\,\mathrm{s})$, upper branch inserted voltage equals zero, i.e. all SMs are disconnected, consequently there is no change of SM charge, voltage remains constant. During approximately $t \in [3.35\,\mathrm{s}, 3.4\,\mathrm{s})$, inserted voltage is rising, while upper branch current is positive, charging upper SMs, leading to positive Δv_{SM} and rise in SM voltage. Control action cannot discharge the HB SM under these conditions. At $t = 3.4\,\mathrm{s}$, branch current crosses zero becoming negative. As instantaneous branch power (1) is negative, SMs are being discharged until $t = 3.44\,\mathrm{s}$. Lower branch can be analyzed in the same manner.

C. Grid-side VS PHSP operation

AFE MMC stage operation sequence, following test scenario (Fig. 5), is presented in Fig. 10. Correct active and reactive power tracking is performed. DC link voltage is correctly controlled (Fig. 7). Capacitor voltage ripple is stable across the operating range, with transients occurring at step change of DC current. In case constant torque is required throughout the zero crossing, this must be taken into account when dimensioning SM capacitance value.

D. LVRT

PHSP response to the most severe LVRT profile defined for Type 2 generating facility in [15], is presented in Fig. 11. Immediately upon fault occurrence, WRSM torque reference is driven to zero. Machine torque control reduces torque output from $0.9\,\mathrm{pu}$ to $0\,\mathrm{pu}$ in $5\,\mathrm{ms}$. For converter parameters in Tab. III, as PSC-PWM is used, apparent switching frequency of $f_{\mathrm{app}} = N_{\mathrm{SM}} f_{\mathrm{sw}} \approx 16\,\mathrm{kHz}$ leads to theoretical current, i.e. torque, control bandwidth of $10T_{\mathrm{app}} = 625\,\mu\mathrm{s}$. A speed deviation (acceleration) from reference is observed upon removal of WRSM torque. In higher-inertia systems, this deviation can be less significant. In any case, as hydraulic system dynamics is decoupled from the grid, these mismatches are perfectly acceptable. On the grid side, AFE stage utilizes full current capacity for reactive current support to the grid. As grid voltage gradually recovers, active energy delivery is resumed.

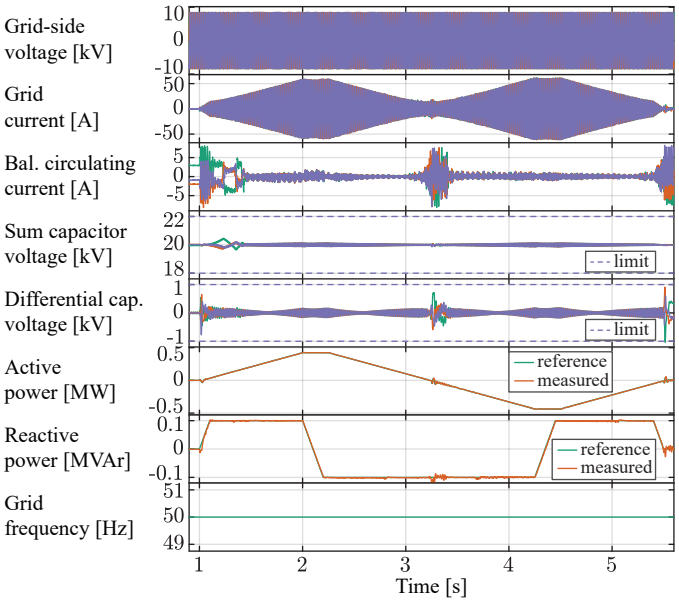

Fig. 10: Grid-side MMC full cycle of opeartion according to the test scenario of Fig. 5.

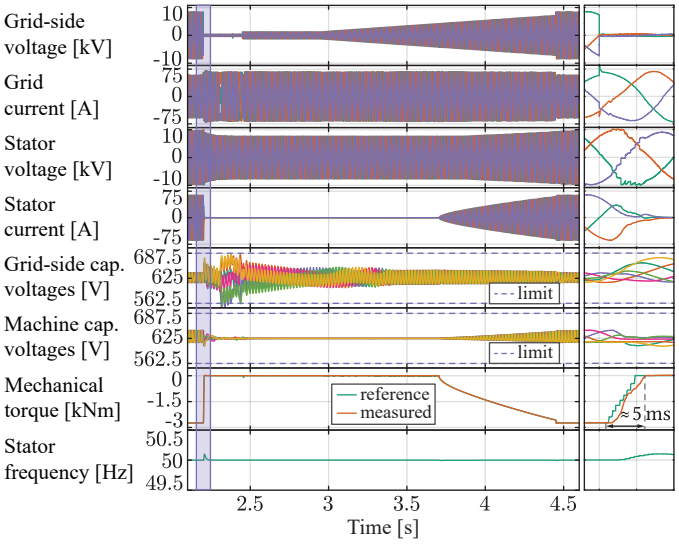

Fig. 11: LVRT sequence of operation according to worst case scenario defined in Fig. 6. Highlighted section is zoomed in.

Conclusion

In the power system with ever increasing share of RES, there is an enormous potential in retrofitting existing reliable PHSPs into highly flexible VS units for advanced grid support. It has been shown that variable-DC-link-operated MMC offers CM-free drive operation over the entire frequency range, while existing studies addressed limited frequency range and open-loop machine control. Full PHSP operating range, under rated torque, including zero-crossing in turbine/pump operation mode switch-over was analyzed. Grid-side fault behaviour is also addressed in terms of PHSP response. Concerning SM capacitance dimensioning, simulation results show that, starting from stored energy requirement of rated-frequency MMC operating point, varying the DC link voltage, the converter can be operated over the entire frequency range, at rated machine torque, while keeping SM voltage ripple within the same design limits.

Acknowledgment

This work has been supported by Innosuisse – Swiss Innovation Agency, under the project No 25109.1 PFEN-IW.

References

[1] J. Pinto, J. De Sousa, and M. V. Neves, "The value of a pumping-hydro generator in a system with increasing integration of wind power," in *2011 8th International Conference on the European Energy Market, EEM 11*, no. May, 2011, pp. 306–311.

[2] M. Valavi and A. Nysveen, "Variable-Speed Operation of Hydropower Plants," *IEEE Industry Applications Magazine*, vol. 24, no. 5, pp. 18–27, 2018.

[3] A. Iwadachi, K. Tani, and K. Aguro, "The design of adjustable-speed pump-turbine modified from existing constant-speed on Okutataragi Power Station," *2016 19th International Conference on Electrical Machines and Systems (ICEMS)*, pp. 1–4, 2016.

[4] A. Vargas-Serrano, A. Hamann, S. Hedtke, C. M. Franck, and G. Hug, "Economic benefit analysis of retrofitting a fixed-speed pumped storage hydropower plant with an adjustable-speed machine," in *2017 IEEE Manchester PowerTech*. IEEE, jun 2017, pp. 1–6.

[5] H. Schlunegger, "Pumping efficiency - A 100 MW converter for the Grimsel 2 pumped storage plant," *ABB Review*, vol. 14, no. 2, pp. 42–47, 2014.

[6] International Hydropower Association, "2019 hydropower status report," 2019. [Online]. Available: https://www.hydropower.org/status2019

[7] M. Basić, P. C. O. Silva, and D. Dujić, "High Power Electronics Innovation Perspectives for Pumped Storage Power Plants," in *2018 Hydro conference*, oct 2018.

[8] M. Vasiladiotis, R. Baumann, C. Haderli, and J. Steinke, "IGCT-Based Direct AC/AC Modular Multilevel Converters for Pumped Hydro Storage Plants," in *2018 IEEE Energy Conversion Congress and Exposition (ECCE)*. IEEE, sep 2018, pp. 4837–4844.

[9] A. J. Korn, M. Winkelnkemper, and P. Steimer, "Low output frequency operation of the Modular Multi-Level Converter," in *2010 IEEE Energy Conversion Congress and Exposition*. IEEE, sep 2010, pp. 3993–3997.

[10] B. Li, S. Zhou, D. Xu, S. J. Finney, and B. W. Williams, "A Hybrid Modular Multilevel Converter for Medium-Voltage Variable-Speed Motor Drives," *IEEE Transactions on Power Electronics*, vol. 32, no. 6, pp. 4619–4630, 2017.

[11] S. Sau, S. Karmakar, and B. G. Fernandes, "Reduction of capacitor ripple voltage and current in Modular Multilevel Converter based variable speed drives," *2017 IEEE 3rd International Future Energy Electronics Conference and ECCE Asia, IFEEC - ECCE Asia 2017*, pp. 1451–1456, 2017.

[12] M. Guan, B. Li, S. Zhou, Z. Xu, and D. Xu, "Back-To-back hybrid modular multilevel converters for ac motor drive," *Proceedings IECON 2017 - 43rd Annual Conference of the IEEE Industrial Electronics Society*, vol. 2017-Janua, pp. 1822–1827, 2017.

[13] S. Sau and B. G. Fernandes, "Modular multilevel converter based variable speed drives with constant capacitor ripple voltage for wide speed range," in *IECON 2017 - 43rd Annual Conference of the IEEE Industrial Electronics Society*, vol. 66, no. 5. IEEE, oct 2017, pp. 2073–2078.

[14] Y. Pannatier, B. Kawkabani, C. Nicolet, J. J. Simond, A. Schwery, and P. Allenbach, "Investigation of control strategies for variable-speed pump-turbine units by using a simplified model of the converters," *IEEE Transactions on Industrial Electronics*, vol. 57, no. 9, pp. 3039–3049, 2010.

[15] European Union, "Commission Regulation (EU) 2016/631 of 14 April 2016 establishing a network code on requirements for grid connection of generators," *Official Journal of the European Union*, vol. 59, 2016. [Online]. Available: https://eur-lex.europa.eu/legal-content/EN/TXT/PDF/?uri=OJ:L:2016:112:FULL&from=EN

[16] M. Basic, S. Milovanovic, and D. Dujic, "Comparison of two Modular Multilevel Converter Internal Energy Balancing Methods," in *2019 20th International Symposium on Power Electronics (Ee)*. IEEE, oct 2019, pp. 1–8.